High Q Chalcogenide Photonic Crystal Nanobeam Cavities

Mingyue Zhao, Zhen Yang, Rizhen Zhang, Jiajiu Zheng, Peipeng Xu, Wei Zhang, Shixun Dai, Rongping Wang, and Arka Majumdar, *Member, IEEE*

***Abstract*— We report high quality (Q) photonic crystal (PhC) nanobeam cavities in the chalcogenide glass $Ge_{28}Sb_{12}Se_{60}$ near 1550 nm wavelength. By optimizing the structure of the PhC cavity, an ultra-high Q factor as large as 5×10^6 is predicted by simulation, and up to 1.2×10^4 is measured in the experiment. Such high-Q cavities in this strongly nonlinear material create an attractive platform for compact, ultrafast all-optical switches.**

***Index Terms*— Integrated optics, photonic crystal, chalcogenide glasses, optical switches.**

I. Introduction

PHOTONIC crystal (PhC) nanocavities with a high quality (Q) factor and low mode volume (V) are of great importance in various applications [1], [2], such as ultra-low energy switching and modulation [3]–[5], sensing [6], [7], and cavity quantum electrodynamics [8]–[10]. While the highest Q factors have been reported in 2D planar PhC cavities, nanobeam cavities (one-dimensional PhC cavities) have attracted much attention [11]–[13], because they can achieve large Q factors in addition to offering design flexibility and relatively simple fabrication, small size, and the ability to confine light in material systems with index contrasts too low to support 2D photonic bandgaps [14]–[17]. Additionally, such nano-beam cavities are easier to be connected or coupled with gratings, waveguides, and other nanophotonic resonators, such as microring resonator [18].

Bistable optical switching in a PhC resonant cavity is particularly attractive because they can be driven with an extremely low input power (scaled as V/Q^2) for all-optical signal processing [5], [19]–[21]. The refractive index modulation via nonlinear optical effects such as thermo-optic (TO) effect [22], [23], carrier-induced effect [3]–[5], and Kerr effect [24]–[26] changes the cavity resonance. If the resonance change increases the effect of the index modulation, a positive feedback can be established resulting in optical bistability in a microcavity. The TO effect can be easily induced but suffer from the slow speed in the megahertz range, which is not useful for high-speed signal processing. On the other hand, carrier-induced effect, including two-photon absorption (TPA) and free-carrier dispersion, are always accompanied by high absorption loss, which significantly degrades the device transmittance. Kerr effect is carrier-free and is regarded as one of the most promising routes due to its instantaneous response and low optical loss. Utilizing its excellent features, optical switches and memories based on Kerr effect have been investigated both theoretically and experimentally [19], [25]–[27].

In spite of being a mature nonlinear photonics material, silicon shows significant TPA and free carrier absorption (FCA), which can degrade the performance of an optical switch at high-bit rates. Chalcogenide glasses (ChGs) are considered a promising material system instead of silicon to realize bistable switching as they afford low TPA and negligible FCA [28], as well as exhibit remarkable electrical and optical properties [29]. First, the linear absorption losses of ChGs are low over a wide wavelength range (up to $\sim 20\mu$m) with the relatively high refractive index ($n = 2 \sim 3$). Moreover, ChGs exhibit exceptionally high optical nonlinearity (Kerr, Raman and Brillouin coefficients) between two to three orders of magnitude greater than silica and comparable or superior to silicon [30]–[32], leading to numerous applications of all-optical signal processing, including optical interconnects [33], wavelength conversion [34], and supercontinuum generation [35], [36]. Several PhC cavities in chalcogenide glass have been demonstrated. White *et al.* [37] reported the first demonstration of 1D PhC nanocavities in chalcogenide glass $Ge_{11.5}As_{24}Se_{64.5}$ with the Q factor of 2.2×10^4. Gai *et al.* [38] designed and fabricated a 2-D photonic crystal heterostructure cavity in $Ge_{11.5}As_{24}Se_{64.5}$ with a high intrinsic $Q > 7.6 \times 10^5$. Although these cavities exhibit good performance,

Manuscript received November 14, 2020; revised January 12, 2021; accepted February 9, 2021. Date of publication February 12, 2021; date of current version April 26, 2021. This work was supported in part by the National Natural Science Foundation of China under Grant 61875099, in part by the Natural Science Foundation of Zhejiang Province under Grant LY18F050005 and Grant LGJ18F050001, in part by the Natural Science Foundation of Ningbo under Grant 202003N4007, in part by the Grant NSF-EFRI-1640986, in part by the Grant NSF-DMR-2003509, in part by the ONR-YIP Award, and in part by the K. C. Wong Magna Fund at Ningbo University. *(Corresponding authors: Peipeng Xu; Arka Majumdar.)*

Mingyue Zhao, Zhen Yang, Rizhen Zhang, Peipeng Xu, Wei Zhang, Shixun Dai, and Rongping Wang are with the Faculty of Electrical Engineering and Computer Science, Ningbo University, Ningbo 315211, China, and also with the Key Laboratory of Photoelectric Detection Materials and Devices of Zhejiang Province, Ningbo University, Ningbo 315211, China (e-mail: 1811082138@nbu.edu.cn; 1901100011@nbu.edu.cn; 1911082132@nbu.edu.cn; xupeipeng@nbu.edu.cn; zhangwei3@nbu.edu.cn; daishixun@nbu.edu.cn; wangrongping@nbu.edu.cn).

Jiajiu Zheng is with the Department of Electrical and Computer Engineering, University of Washington, Seattle, WA 98195 USA (e-mail: jjzno1@uw.edu).

Arka Majumdar is with the Department of Electrical and Computer Engineering, University of Washington, Seattle, WA 98195 USA, and also with the Department of Physics, University of Washington, Seattle, WA 98195 USA (e-mail: arka@uw.edu).

Color versions of one or more figures in this letter are available at https://doi.org/10.1109/LPT.2021.3059040.

Digital Object Identifier 10.1109/LPT.2021.3059040

the As-containing chalcogenide glasses are toxic, which is not conductive to large-scale fabrication. We note that silicon nitride is another promising material for nonlinear optics, but the low index of the material (n∼2) often poses challenges to be integrated with substrates with high index.

In this work, utilizing $Ge_{28}Sb_{12}Se_{60}$, one of the nontoxic ChGs, we present a design and fabrication of a high Q nanobeam cavity, which consists of a series of periodically arranged elliptical holes. In previous ChG photonics studies, the ternary and nontoxic ChG such as Ge–Sb–Se and Ge-Sb-S have attracted less attention than the As-containing and binary ChG such as As_2S_3 and As_2Se_3. This is mainly because the composition deviation of ternary films prepared by thermal evaporation is relatively large, which is not conductive to nonlinear photonics application. In recent years, people have made great progress in ternary ChG film preparation. For example, Chen *et al.* [39] successfully deposited $Ge_{28}Sb_{12}Se_{60}$ thin films with compositions close to the glassy target on glass slides at room temperature by thermal evaporation. Compared with As_2S_3 glass, which has been a major workhorse for all-optical devices to date [40], $Ge_{28}Sb_{12}Se_{60}$ has a higher linear refractive index (∼2.8 compared with ∼2.3 for As_2S_3) which leads to better mode confinement. By optimizing the size of elliptical holes, an ultra-high Q factor as large as 5×10^6 is predicted by simulation, and up to 1.2×10^4 is measured in experiment. Thanks to the high Q factor, high nonlinear coefficients and small mode-volume ($V \sim 1.2(\lambda/n)^3$), the reported ChGs nanobeam cavity shows great potential to demonstrate low-power, ultrafast switching, and optical signal processing.

II. Design and Analysis

The structure based on the $Ge_{28}Sb_{12}Se_{60}$ platform is a dielectric mode elliptical-hole 1D PhC cavity, which includes a 300 nm thick $Ge_{28}Sb_{12}Se_{60}$ device layer and a 2 μm thick buried silicon dioxide layer. The refractive index of the $Ge_{28}Sb_{12}Se_{60}$ and silica buffer layer are 2.83 and 1.44, respectively, at a wavelength of 1550 nm. The upper cladding is set to be air. Figure 1(a) presents the schematic of the chalcogenide PhC nanobeam cavity, consisting of a 1D array of elliptical holes. From the top view of the cavity (Fig. 1(b)), the radius of the horizontal and the vertical axis of each elliptical cell are R_x and R_y, respectively. To minimize scattering loss in the propagation direction x, we keep the period a, i.e., the transverse (x-axis) distance between the elliptical holes, constant to ensure optical phase matching between adjacent unit cells. To achieve a preferred Gaussian field profile, Quan *et al.* proposed an efficient method by introducing a linearly increased attenuation of the electromagnetic field from the center holes to the edge holes of the PhC cavity [11], [41]. Here, the radius of the vertical axis of the elliptical holes are modulated from $R_y(0)$ in the center to $R_y(n_{\max})$ on the each sides parabolically: $R_y(n) = R_y(0) + \frac{(n-1)^2}{(n_{\max}-1)^2} \times \left[R_y(n_{\max}) - R_y(0)\right]$, n increases from 1 to $n_{\max}$. Three-dimensional finite-difference-time-domain (3D-FDTD) method is used to simulate the photonic band structure, and finite-element-methods (FEMs) are used to simulate the field distribution of the PhC cavity with patterned elliptical

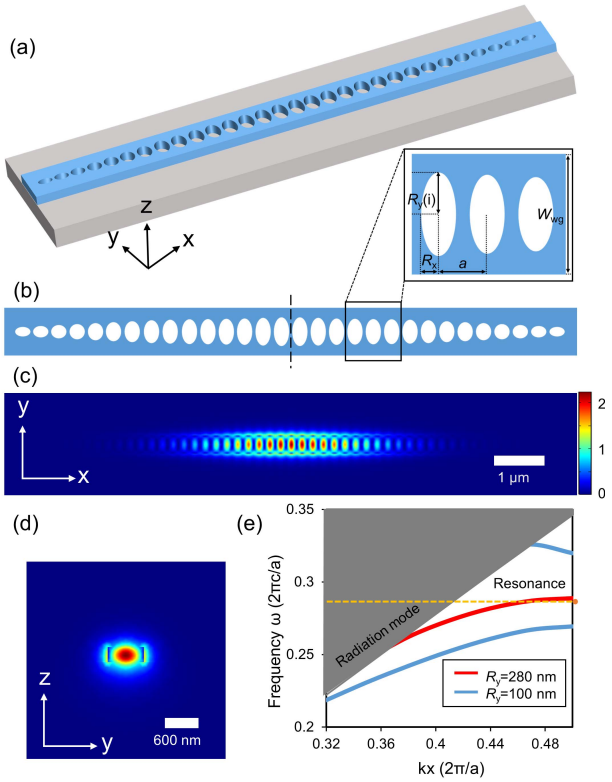

Fig. 1. (a) Schematic of the proposed PhC nanobeam cavity. (b) Top view of the device. Inset: zoom-in view of the framed part. The electric field distribution from (c) top view (xy plane) and (d) side view (yz plane) at the center of the cavity. (e) The calculated band diagram of the unit cell with $R_y = 280$ nm (red curve) and $R_y = 100$ nm (blue curve), the orange circle indicates the resonant frequency, and the gray region indicates the radiation modes.

holes. Figures 1(c) and 1(d) show the electric field distribution of the PhC cavity, from the top (xy-plane) and the side (yz-plane), respectively. We find that the fundamental TE mode of the cavity is a dielectric mode in which the optical field dominantly is located inside the high index chalcogenide region. In simulations, there are 25 elliptical unit cells in the taper region on each side of the PhC cavity, and only part of the cells is shown in the figure. Figure 1(e) shows the TE band diagrams of the PhC cavity, which are calculated from series band structure simulations with Bloch boundary conditions. The red curve shows the band diagram of $R_y(0) = 280$ nm (the vertical axis radius of the center ellipse hole), while the blue one indicates the band diagram of $R_y(n_{\max}) = 100$ nm (the vertical axis radius of the edge elliptical hole). The resonance frequency of the cavity mode (the dot and dashed line in Fig. 1(e)) is slightly lower than the dielectric band edge of the elliptical cell with $R_y(0) = 280$ nm, which is consistent with the perturbation theory described by Quan and Loncar [41]. To keep the resonant wavelength of the cavity near 1550 nm, the period is chosen as $a = 440$ nm, and the waveguide width is chosen as $W = 720$ nm.

From the above optimization and analysis, the geometric parameters of the PhC nanobeam cavity are summarized to be: $a = 440$ nm, $W = 720$ nm, $R_y(0) = 280$ nm, $R_y(n_{\max}) = 100$ nm, $R_x = 160$ nm, and $N_{\text{mirror}} = 25$ on each side. With these parameters, most of the electric field of resonant mode is confined in the high index chalcogenide region between

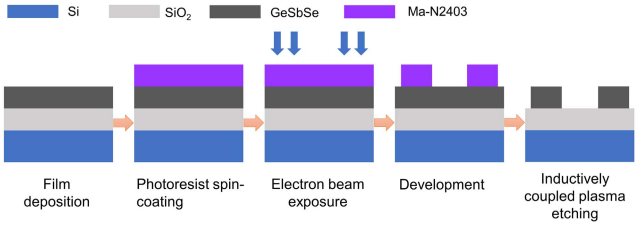

Fig. 2. The fabrication process of the ChGs PhC nanobeam cavity.

the elliptical holes of the PhC cavity. Further simulations by the finite element method show that the cavity mode exhibits a radiation-limited optical Q as high as 5×10^6, with an effective mode volume as small as $\sim 1.2(\lambda/n)^3$ (defined by $V = \int dV\varepsilon |E|^2/(\varepsilon |E|^2)_{\max}$, where E is the electric field and ε is the permittivity). The resonant wavelength of the fundamental mode used for the cavities is 1531.7 nm.

III. Fabrication and Characterization

The designed ChGs PhC nanobeam cavity was fabricated on a chalcogenide glass platform using the following process as illustrated in Fig. 2. First, a 300 nm thick film of $Ge_{28}Sb_{12}Se_{60}$ glass was thermally deposited onto a 2-μm oxidized silicon wafer as a substrate. Then a negative tone electron beam resist (MA-N 2403) was spin-coated onto the $Ge_{28}Sb_{12}Se_{60}$ wafer at 4000 rpm, and the thickness of the MA-N 2403 film was 330 nm. Electron beam lithography (Raith Eline Plus) is used to define patterns at an acceleration voltage of 30 KV, and then developed in MA-D 525 solution. Inductively coupled plasma etching using a gas mixture of CHF_3 and CF_4 was then used to transfer the PhC pattern into the chalcogenide film. To remove the remaining resist, we first put the sample into the ICP etcher, and bombard it with the gas mixture $CHF_3/AR/O_2$ for 20s, then shake it with a 1-Methyl-2-pyrrolidone on a 70 °C shaker for 3 minutes, and finally rinsed in DI water.

Figures 3(a) and 3(b) show the scanning electron micrographs (SEMs) of the fabricated cavity and the zoom in view of the elliptical holes at the end of the PhC cavity, respectively. The minimum feature size of the cavity is ~80 nm, which shows clearly well-defined and uniform elliptical holes and an accurately patterned lattice structure. To characterize the performance of the device, we measured the transmission spectrum of resonators using a vertical fiber coupling setup. Grating couplers were fabricated at each input and output port for chip-fiber coupling and polarization selectivity, as shown in Fig. 3(c). The TE polarization grating coupler was designed with a fixed duty cycle of 70%, a period of 920 nm, and a fully etch depth of 300 nm. SMF-28e single-mode fibers were aligned to the grating couplers at an incident angle of 12°. A tunable laser (Santec TSL-550) with a wavelength ranging from 1500 to 1630 nm is used as the light source. The polarization of the input light was controlled to match the fundamental quasi-TE mode of the waveguide by a manual fiber polarization controller (Thorlabs FPC562). The light was collected on the other side of the waveguides into a high-resolution and sensitivity power meter ((UC Instruments UC8820) via single-mode fibers (SMFs).

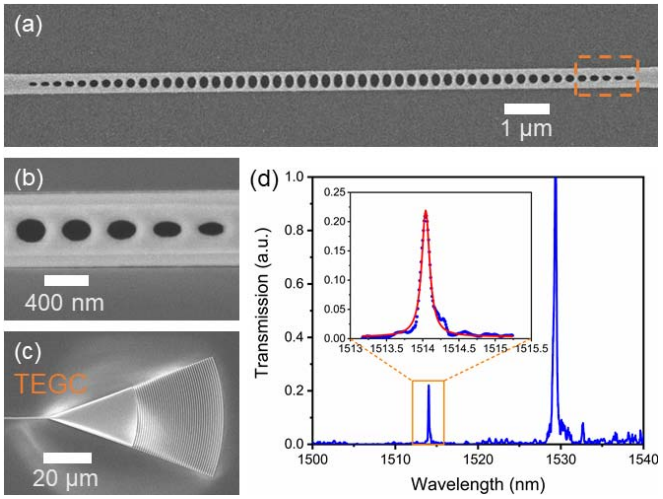

Fig. 3. (a), (b) SEM of the device and enlarged view of the dotted frame on the right end of the device. (c) SEM of the TE polarization grating coupler. (d) The measured transmission spectrum of the nanobeam cavity in air. The inset shows the fit to Lorentzian lineshape for the resonance. (Q~ 1.2×10^4).

Figure 3(d) presents the transmission spectrum of the device normalized by the peak resonance transmission. The cavity has a fundamental mode resonance at 1514.1 nm. The full width at half maximum (FWHM) for the Lorentz fit of the measured result is $\sim$ 126 pm, which indicates a high Q factor of $\sim 1.2 \times 10^4$. The extinction ratio is larger than 15 dB. The degradation of the Q factor compared with the design is mainly due to the sidewall scattering loss and the inhomogeneity of the shape of the holes caused by the dry etching process. Further improvement of Q factor may be achieved by optimizing the fabrication processes. In addition, we found that the PhC cavity supports higher-order resonance modes, and the higher-order mode can be well separated from the fundamental mode. The Q value of the higher-order mode is significantly smaller than the fundamental one.

IV. Conclusion

We have demonstrated the design and fabrication of a high Q PhC nanobeam cavity on $Ge_{28}Sb_{12}Se_{60}$ platform. Benefitting from the Gaussian-shaped field profile within the cavity, an optimized Q factor of $\sim 5 \times 10^6$ in simulations and $\sim 1.2 \times 10^4$ in the experiment has been achieved. Furthermore, the total size of the nanobeam is only $24 \times 0.72\mu m^2$. The availability of such compact, high Q and high nonlinear nanobeam cavity makes them excellent candidates to low-power, ultrafast switching, and optical signal processing.

References

[1] Y. Akahane, T. Asano, B.-S. Song, and S. Noda, "High-Q photonic nanocavity in a two-dimensional photonic crystal," *Nature*, vol. 425, no. 6961, pp. 944–947, Oct. 2003.
[2] B.-S. Song, S. Noda, T. Asano, and Y. Akahane, "Ultra-high-Q photonic double-heterostructure nanocavity," *Nature Mater.*, vol. 4, no. 3, pp. 207–210, Feb. 2005.
[3] K. Nozaki *et al.*, "Sub-femtojoule all-optical switching using a photonic-crystal nanocavity," *Nature Photon.*, vol. 4, no. 7, pp. 477–483, May 2010.
[4] K. Nozaki *et al.*, "Ultralow-power all-optical RAM based on nanocavities," *Nature Photon.*, vol. 6, no. 4, pp. 248–252, Feb. 2012.

[5] T. Tanabe, M. Notomi, S. Mitsugi, A. Shinya, and E. Kuramochi, "Fast bistable all-optical switch and memory on a silicon photonic crystal on-chip," *Opt. Lett.*, vol. 30, no. 19, pp. 2575–2577, Oct. 2005.

[6] B. Wang, M. A. Dündar, R. Nötzel, F. Karouta, S. He, and R. W. van der Heijden, "Photonic crystal slot nanobeam slow light waveguides for refractive index sensing," *Appl. Phys. Lett.*, vol. 97, no. 15, Oct. 2010, Art. no. 151105.

[7] P. Xu, J. Zheng, J. Zhou, Y. Chen, C. Zou, and A. Majumdar, "Multi-slot photonic crystal cavities for high-sensitivity refractive index sensing," *Opt. Exp.*, vol. 27, no. 3, pp. 3609–3616, Feb. 2019.

[8] T. Yoshie *et al.*, "Vacuum Rabi splitting with a single quantum dot in a photonic crystal nanocavity," *Nature*, vol. 432, no. 7014, pp. 200–203, Nov. 2004.

[9] D. Englund, A. Majumdar, M. Bajcsy, A. Faraon, P. Petroff, and J. Vučković, "Ultrafast photon-photon interaction in a strongly coupled quantum dot-cavity system," *Phys. Rev. Lett.*, vol. 108, no. 9, Mar. 2012, Art. no. 093604.

[10] R. Bose, D. Sridharan, H. Kim, G. S. Solomon, and E. Waks, "Low-photon-number optical switching with a single quantum dot coupled to a photonic crystal cavity," *Phys. Rev. Lett.*, vol. 108, no. 22, May 2012, Art. no. 227402.

[11] Q. Quan, P. B. Deotare, and M. Loncar, "Photonic crystal nanobeam cavity strongly coupled to the feeding waveguide," *Appl. Phys. Lett.*, vol. 96, no. 20, May 2010, Art. no. 203102.

[12] M. Notomi, E. Kuramochi, and H. Taniyama, "Ultrahigh-Q nanocavity with 1D photonic gap," *Opt. Exp.*, vol. 16, no. 15, pp. 11095–11102, Jul. 2008.

[13] P. Xu, K. Yao, J. Zheng, X. Guan, and Y. Shi, "Slotted photonic crystal nanobeam cavity with parabolic modulated width stack for refractive index sensing," *Opt. Exp.*, vol. 21, no. 22, pp. 26908–26913, Nov. 2013.

[14] Y. Gong and J. Vučković, "Photonic crystal cavities in silicon dioxide," *Appl. Phys. Lett.*, vol. 96, no. 3, Jan. 2010, Art. no. 031107.

[15] Q. Quan, I. B. Burgess, S. K. Y. Tang, D. L. Floyd, and M. Loncar, "High-Q, low index-contrast polymeric photonic crystal nanobeam cavities," *Opt. Exp.*, vol. 19, no. 22, pp. 22191–22197, Oct. 2011.

[16] T. K. Fryett, Y. Chen, J. Whitehead, Z. M. Peycke, X. Xu, and A. Majumdar, "Encapsulated silicon nitride nanobeam cavity for hybrid nanophotonics," *ACS Photon.*, vol. 5, no. 6, pp. 2176–2181, Jun. 2018.

[17] D. Freeman *et al.*, "Chalcogenide glass photonic crystals," *Photon. Nanostruct.*, vol. 6, no. 1, pp. 3–11, Apr. 2008.

[18] K. C. Smith, Y. Chen, A. Majumdar, and D. J. Masiello, "Active tuning of hybridized modes in a heterogeneous photonic molecule," *Phys. Rev. Appl.*, vol. 13, no. 4, Apr. 2020, Art. no. 044041.

[19] T. Tanabe, M. Notomi, S. Mitsugi, A. Shinya, and E. Kuramochi, "All-optical switches on a silicon chip realized using photonic crystal nanocavities," *Appl. Phys. Lett.*, vol. 87, no. 15, Oct. 2005, Art. no. 151112.

[20] R. Trivedi, U. K. Khankhoje, and A. Majumdar, "Cavity-enhanced second-order nonlinear photonic logic circuits," *Phys. Rev. Appl.*, vol. 5, no. 5, May 2016, Art. no. 054001.

[21] T. K. Fryett, C. M. Dodson, and A. Majumdar, "Cavity enhanced nonlinear optics for few photon optical bistability," *Opt. Exp.*, vol. 23, no. 12, pp. 16246–16255, Jun. 2015.

[22] M. Notomi, A. Shinya, S. Mitsugi, G. Kira, E. Kuramochi, and T. Tanabe, "Optical bistable switching action of Si high-Q photonic-crystal nanocavities," *Opt. Exp.*, vol. 13, no. 7, pp. 2678–2687, Mar. 2005.

[23] M. W. Lee *et al.*, "Photosensitive and thermal nonlinear effects in chalcogenide photonic crystal cavities," *Opt. Exp.*, vol. 18, no. 25, pp. 26695–26703, Dec. 2010.

[24] M. Pöllinger and A. Rauschenbeutel, "All-optical signal processing at ultra-low powers in bottle microresonators using the Kerr effect," *Opt. Exp.*, vol. 18, no. 17, pp. 17764–17775, Aug. 2010.

[25] V. Eckhouse, I. Cestier, G. Eisenstein, S. Combrié, G. Lehoucq, and A. De Rossi, "Kerr-induced all-optical switching in a GaInP photonic crystal Fabry–Pérot resonator," *Opt. Exp.*, vol. 20, no. 8, pp. 8524–8534, Apr. 2012.

[26] M. F. Yanik, S. Fan, and M. Soljačić, "High-contrast all-optical bistable switching in photonic crystal microcavities," *Appl. Phys. Lett.*, vol. 83, no. 14, pp. 2739–2741, Oct. 2003.

[27] W. Yoshiki and T. Tanabe, "Performance of Kerr bistable memory in silicon nitride microring and silica microtoroid," *Jpn. J. Appl. Phys.*, vol. 53, no. 12, Nov. 2014, Art. no. 122202.

[28] B. J. Eggleton *et al.*, "Photonic chip based ultrafast optical processing based on high nonlinearity dispersion engineered chalcogenide waveguides," *Laser Photon. Rev.*, vol. 6, no. 1, pp. 97–114, Jan. 2012.

[29] B. J. Eggleton, B. Luther-Davies, and K. Richardson, "Chalcogenide photonics," *Nature Photon.*, vol. 5, no. 3, pp. 141–148, Feb. 2011.

[30] G. Lenz *et al.*, "Large Kerr effect in bulk Se-based chalcogenide glasses," *Opt. Lett.*, vol. 25, no. 4, pp. 254–256, Feb. 2000.

[31] V. G. Ta'eed *et al.*, "Ultrafast all-optical chalcogenide glass photonic circuits," *Opt. Exp.*, vol. 15, no. 15, pp. 9205–9221, Jul. 2007.

[32] B. J. Eggleton, C. G. Poulton, and R. Pant, "Inducing and harnessing stimulated Brillouin scattering in photonic integrated circuits," *Adv. Opt. Photon.*, vol. 5, no. 4, pp. 536–587, Dec. 2013.

[33] T. D. Vo *et al.*, "Photonic chip based transmitter optimization and receiver demultiplexing of a 1.28 Tbit/s OTDM signal," *Opt. Exp.*, vol. 18, no. 16, pp. 17252–17261, Aug. 2010.

[34] V. G. Ta'eed *et al.*, "All optical wavelength conversion via cross phase modulation in chalcogenide glass rib waveguides," *Opt. Exp.*, vol. 14, no. 23, pp. 11242–11247, Oct. 2006.

[35] M. R. E. Lamont, B. Luther-Davies, D.-Y. Choi, S. Madden, and B. J. Eggleton, "Supercontinuum generation in dispersion engineered highly nonlinear ($\gamma = 10$/W/m) As_2S_3 chalcogenide planar waveguide," *Opt. Exp.*, vol. 16, no. 19, pp. 14938–14944, Sep. 2008.

[36] Y. Yu *et al.*, "Experimental demonstration of linearly polarized 2–10 μm supercontinuum generation in a chalcogenide rib waveguide," *Opt. Lett.*, vol. 41, no. 5, pp. 958–961, Mar. 2016.

[37] T. P. White, X. Gai, S. Madden, D.-Y. Choi, S. Debbarma, and B. Luther-Davies, "Bistable switching in chalcogenide 1D photonic crystal nanocavities," in *Proc. CLEO/Europe EQEC*, May 2011, pp. 1–4.

[38] X. Gai, B. Luther-Davies, and T. P. White, "Photonic crystal nanocavities fabricated from chalcogenide glass fully embedded in an index-matched cladding with a high Q-factor (>750,000)," *Opt. Exp.*, vol. 20, no. 14, pp. 15503–15515, Jul. 2012.

[39] Y. Chen *et al.*, "Optical and structural properties of Ge–Sb–Se thin films fabricated by sputtering and thermal evaporation," *J. Alloys Compounds*, vol. 548, pp. 155–160, Jan. 2013.

[40] S. J. Madden *et al.*, "Long, low loss etched As_2S_3 chalcogenide waveguides for all-optical signal regeneration," *Opt. Exp.*, vol. 15, no. 22, pp. 14414–14421, Oct. 2007.

[41] Q. Quan and M. Loncar, "Deterministic design of wavelength scale, ultra-high Q photonic crystal nanobeam cavities," *Opt. Exp.*, vol. 19, no. 19, pp. 18529–18542, Sep. 2011.